universe

MDPI

Article

Where to Search for Supermassive Binary Black Holes

Paola Marziani [1,*], Edi Bon [2], Natasa Bon [2] and Mauro D'Onofrio [1,3]

[1] National Institute for Astrophysics (INAF), Astronomical Observatory of Padova, IT-35122 Padova, Italy; mauro.donofrio@unipd.it
[2] Astronomical Observatory Belgrade, Volgina 7, 11060 Belgrade, Serbia; ebon@aob.rs (E.B.); nbon@aob.rs (N.B.)
[3] Department of Physics and Astronomy, University of Padua, IT-35122 Padova, Italy
* Correspondence: paola.marziani@inaf.it

Abstract: Supermassive binary black holes (SMBBHs) are the anticipated byproducts of galaxy mergers and play a pivotal role in shaping galaxy evolution, gravitational wave emissions, and accretion physics. Despite their theoretical prevalence, direct observational evidence for SMBBHs remains elusive, with only a handful of candidates identified to date. This paper explores optimal strategies and key environments for locating SMBBHs, focusing on observational signatures in the broad Balmer lines. We present a preliminary analysis on a flux-limited sample of sources belonging to an evolved spectral type along the quasar main sequence, and we discuss the spectroscopic clues indicative of binary activity and highlight the critical role of time-domain spectroscopic surveys in uncovering periodic variability linked to binary systems.

Keywords: galaxies; active galaxies; quasars; emission-lines; evolution of galaxies; black hole physics; supermassive binary black holes; accretion; line formation

check for updates

Academic Editor: Yongquan Xue

Received: 22 January 2025
Revised: 12 February 2025
Accepted: 17 February 2025
Published: 21 February 2025

Citation: Marziani, P.; Bon, E.; Bon, N.; D'Onofrio, M. Where to Search for Supermassive Binary Black Holes. *Universe* **2025**, *11*, 76. https://doi.org/10.3390/universe11030076

Copyright: © 2025 by the authors. Licensee MDPI, Basel, Switzerland. This article is an open access article distributed under the terms and conditions of the Creative Commons Attribution (CC BY) license (https://creativecommons.org/licenses/by/4.0/).

1. Introduction

Supermassive black hole binaries (SMBBHs) are an expected consequence of hierarchical galaxy formation. As galaxies merge, their central supermassive black holes (SMBHs), with masses ranging from 10^6–10^9 $M_\odot$, are brought together by dynamical friction and may eventually form a bound binary system [1,2]. SMBBHs are useful for understanding a wide range of astrophysical processes [3], including galaxy evolution, the fueling of active galactic nuclei (AGN), and the generation of low-frequency gravitational waves detectable by pulsar timing arrays (PTAs, [4,5]) and future space-based observatories like LISA [6–8]. Despite their theoretical significance, the observational evidence for SMBBHs remains sparse, with only a handful of candidates identified through periodicity in AGN light curves, dual-AGN systems, or distinct velocity offsets in emission lines [9–11]. Several claims of periodic behavior were refuted after long-term monitoring [12–14]. Current estimates of the population of SMBBHs vary depending on the assumptions about galaxy merger rates, SMBH masses, and the efficiency of binary coalescence [15]. Models predict that thousands of SMBBHs could exist within the detectable range of PTAs, assuming typical binary separations of 0.1–10 parsecs and orbital periods ranging from months to decades [4,16]. However, the true population remains highly uncertain due to the complex interplay of gas dynamics, stellar interactions, and gravitational wave emission in the binary evolution [17]. Future surveys and gravitational wave observations are expected to provide a more comprehensive census.

The electromagnetic phenomenology of SMBBHs is anything but clear. Previous attempts to identify SMBBHs have resorted to the detection of periodic phenomena involving

photometric and spectroscopic properties. Photometric periodicities can arise from several mechanisms, including the modulation of accretion rates due to the gravitational interaction between the binary components, relativistic Doppler boosting of emission from the mini-disk around one of the black holes, or periodic disruptions of gas streams. Examples include the AGN PG 1302-102, which exhibits quasi-periodic oscillations with a period of approximately 5 years, interpreted as evidence of a binary with a sub-parsec separation [18]. Additional candidates have been identified in large surveys such as the Palomar Transient Factory (PTF) and Zwicky Transient Facility (ZTF) [19–22], where systematic searches for periodic variability in AGN light curves have revealed populations consistent with binary models [23]. Furthermore, irregular photometric dips or flares, potentially linked to gas dynamics in the circum-binary disk or mini-disks, provide complementary evidence for the presence of SMBBHs [10].

The interpretation of quasi-periodic variability as evidence for supermassive black hole binaries (SMBBHs) faces significant challenges, particularly from red noise in AGN light curves. AGNs exhibit stochastic variability across a broad range of timescales, which can produce apparent periodic signals through random fluctuations. This variability is characterized by a power-law power spectral density (PSD), where lower-frequency (longer timescale) variations dominate, often described as red noise. Simulated light curves with red noise properties have been shown to produce spurious periodicities that mimic the signals expected from SMBBHs [24,25]. Criticism of candidates like PG 1302-102, originally proposed as a binary due to its periodic variability [18], highlights the difficulty of distinguishing true periodic signals from statistical artifacts [14]. Rigorous tests, such as the Lomb-Scargle periodogram and wavelet analysis, must account for the PSD of AGN variability to avoid false positives [26]. Long monitoring timescales are essential in verifying periodicity over multiple cycles and rule out red noise as the source of variability. Systematic studies, such as those using Pan-STARRS and ZTF, increasingly incorporate red noise models to refine binary candidates and improve the reliability of photometric searches for SMBBHs [27]. Applying the same criterion customarily used for binary stars (at least three full orbits of monitoring [28]) would imply a monitoring time of several decades, and sufficient data are not yet available for SMBBHs.

Broad emission line profile variability offers a promising avenue for detecting SMBBHs. In a binary system, the orbital motion of the black holes, coupled with their interaction with surrounding gas, can produce periodic changes in the broad-line profiles, such as centroid shifts, line asymmetries, or double peaks. Variability in the broad-line profiles of AGN such as NGC 4151 suggests that gravitational interactions between binary components might influence the emission region [29]. Shen et al. [30] conducted a systematic search for binary SMBHs by examining velocity shifts in broad-line centroids using multi-epoch spectroscopy from the Sloan Digital Sky Survey (SDSS), providing statistical evidence for potential binaries. Simulations further demonstrated that periodic line profile changes (e.g., [31]), including double peaks and shifts, can arise from mini-disks around individual SMBHs in a binary system. However, the exploration of the long-term variability of quasars with double-peaked and peculiar profiles disfavored the idea that periodic changes in the broad Hβ line could be attributed to a SMBBH system [13].

Additional evidence for SMBBHs is arguably based on peculiar broad-line profiles. The broad-line region (BLR) of 1E 1821 + 643 exhibits significant velocity offsets of its broad emission line profiles, with the Hβ line centroid shifted by thousands of kilometers per second relative to the host galaxy's systemic velocity [32]. Such offsets could be interpreted as evidence of a gravitationally bound binary system, where the orbital motion of one black hole contributes to the Doppler shift of the observed emission lines. Alternatively, the velocity shifts could indicate a recoiling black hole, where a gravitational wave "kick"

following a binary black hole merger ejects the remnant black hole at high velocity from the center of the galaxy [32,33]. Both scenarios are considered compelling but remain speculative due to the complex dynamics of the BLR and alternative explanations involving anisotropic gas motion or asymmetric accretion flows. Future multi-wavelength monitoring, including precision radial velocity measurements and time-domain studies, may help distinguish between these interpretations and provide deeper insight into the nature of 1E 1821 + 643.

While observational evidence remains sparse due to the complexity of BLR dynamics and the long orbital timescales of SMBBHs, high-resolution spectroscopic monitoring and advanced time-domain surveys are paving the way for more robust detections. However, interpretation is made more complex by the lack of consensus over the expected phenomenology of emission line profiles. Furthermore, in the case of extreme mass ratio inspirals, a second black hole may not provide a detectable electromagnetic signal, while still perturbing line emission or circum-primary accretion disk.

The previous considerations are meant to stress that an efficient search for SMBBHs should be highly focused. A blind search over the full AGN population will be probably overwhelmed by the red noise characteristics of the light curves and by the lack of contextualization of emission line profile properties. The aim of this note is to point out that there is a well-defined segment of the quasar main sequence where SMBBHs can be more easily detected. We begin by summarizing the concept of the quasar main sequence (MS), a framework that has proven to be an effective tool for organizing the diversity of type-1 AGN (Section 2). From the MS, we focus on a specific spectral type and conduct a detailed analysis of the emission line profiles of the Balmer HI line Hβ and the UV resonance line MgIIλ2800 (Section 2.1). This particular spectral type exhibits several sources with emission line profiles that can be interpreted as being perturbed by the presence of a secondary compact object. Based on this interpretation, we identify a set of promising candidates for further monitoring (Sections 3 and 4) and outline the fundamental multi-messenger characteristics expected of such binary systems (Section 5).

2. The Quasar Main Sequence: A Brief Synopsis

The concept of the main sequence in quasar studies originated from a Principal Component Analysis (PCA) applied to the spectra of Palomar Green quasars, which identified a dominant trend known as Eigenvector 1 (E1; [34]). The E1 revealed an anti-correlation between the strength of the singly ionized iron emission blend centered at λ4570, and the full width at half maximum (FWHM) of Hβ, or alternatively, the peak intensity of [OIII]λ5007. The MS can be represented in a plane where FWHM(Hβ) is plotted against the parameter $R_{\rm FeII}$, defined as the flux ratio F(FeIIλ4570)/F(H$\beta_{\rm BC}$). Figure 1 illustrates the quasar MS in this parameter space. Over time, the MS has been validated and extended from the original sample of 80 objects [34], encompassing now hundreds [35] and tens of thousands of sources [36]. The trends identified in the MS have been linked to the physical properties of the accretion process and outflows, confirmed by multi-frequency data [37–39] and advanced techniques like locally linear embedding in manifold learning [40,41]. The MS captures fundamental correlations related to quasar dynamics, orientation, and the accretion structure.

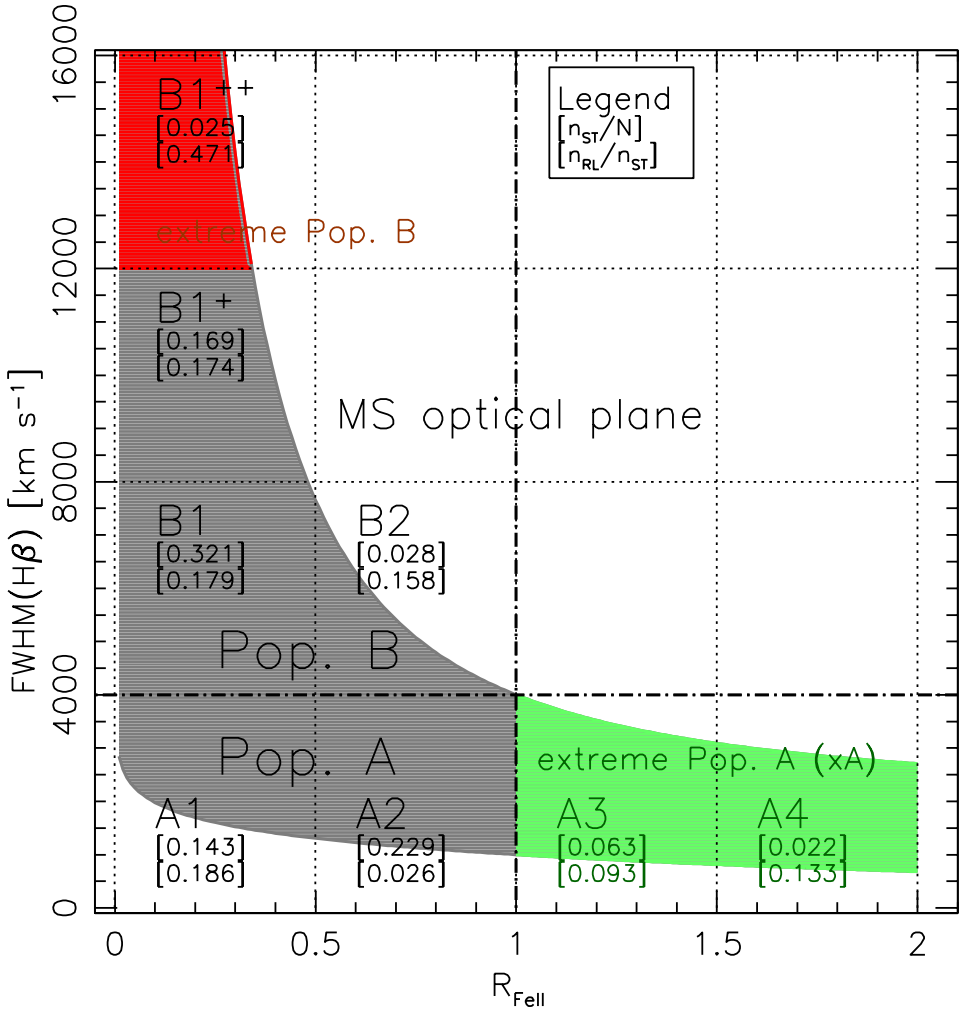


Figure 1. Schematic representation of the optical plane of the quasar main sequence, with the subdivisions into spectral bins clearly marked. The numbers in square brackets beneath each spectral type label indicate the prevalence of the spectral type (number n_{ST} of sources in each spectral type normalized by the number of sources in the full sample), and the fraction of RL (jetted) sources n_{RL}/n_{ST} within each type. The data are from the sample of Marziani et al. [42].

The MS encompasses only type-1 AGN, where broad emission lines are visible, and orientation constraints (angle between the line of sight and the AGN symmetry axis $\theta \lesssim 45$) affect the observed line widths. The parameters FWHM(Hβ) and $R_{\rm FeII}$ are particularly revealing. FeII emission, which spans from the UV to the IR, is largely self-similar in type-1 AGN but varies in relative strength to Hβ, with $R_{\rm FeII}$ values ranging from undetectable to $\gtrsim$2 [37,43], which can be directly linked to Eddington ratio [35,44–46]. The FWHM of Hβ reflects the virialized velocity field of the low-ionization BLR and is influenced by orientation, with the angle θ playing a key role [47–49].

A defining feature of the MS is its "elbow" shape, dividing sources into Population A (Pop. A) and Population B (Pop. B) [37]. Pop. A quasars, characterized by FWHM(Hβ) $\lesssim$4000 km/s, exhibit sharp Hβ profiles, prominent FeII emission, and weak [OIII], while Pop. B quasars, with broader Hβ profiles, display weaker FeII and stronger [OIII] [37]. Additionally, high-ionization lines such as CIV λ1549 show systematic blueshifts relative to narrow low-ionization lines like [OII] λ3727 or Hβ narrow component [50]. These distinctions suggest a heuristic subdivision of the BLR into a virialized low-ionization region, likely associated with the accretion disk, and a wind-dominated high-ionization region, particularly pronounced in extreme Population A (xA) sources where $R_{\rm FeII} > 1$ [51–53].

2.1. A Special Section of the Main Sequence

Extreme Population B sources are characterized by extremely broad Balmer line profiles, with conventional FWHM limits of $\gtrsim$12,000 km s^{-1} or even $\gtrsim$16,000 km s^{-1}. They include only the most extreme cases and occupy the spectral type B1^{++} in Figure 1). A visual inspection shows very broad symmetric profiles (the red wing of Hβ is invariably extended beyond the [OIII]$\lambda\lambda$4959,5007 emission). These sources also exhibit a very low, often undetectable, $R_{\rm FeII}$, in contrast to Population A, where the majority of sources have a measurable $R_{\rm FeII}$. A hallmark of Population B is the pronounced redward asymmetry in low-ionization lines, such as Hβ, a feature well-documented in the literature [35,54–59]. However, the situation for spectral type B1^{++} remains unclear; the MgIIλ2800 and Hβ median spectra show an asymmetry index consistent with a symmetric profile (AI $\approx 0.02 \pm 0.06$ and $\approx 0.04 \pm 0.06$ for the two lines, [42]).

The $R_{\rm FeII}$ parameter, central to the definition of the MS, depends not only on the gas physical conditions but also on chemical abundances. This makes it crucial to understand how metallicity (Z) influences a source location in the optical MS plane [39,60,61]. Another key insight from MS studies is the distinct differences in the prevalence of radio-loud (RL) sources across populations. Extreme Population B hosts the largest fraction of "jetted" sources ($\approx$50% as reported in Figure 1), distinguished from radio-quiet (RQ) ones by their distribution of blueshifts in high-ionization lines. Interestingly, radio-loudness has a minor effect on the low-ionization lines [62,63], while extreme Population A also includes powerful radio emitters, although these objects are likely fundamentally different in nature from the powerful, jetted sources in Population B. The radio-emitting sources of extreme Population A might be dominated by star formation, with the possible contribution of other mechanisms [64–67].

3. Candidate SMBBHs Along the Quasar Main Sequence

Samples and Measurements

The sample of Marziani et al. [42,68] is flux-limited and encompasses 680 objects from the DR7 of the SDSS, in the redshift range $0.4 \leq z \leq 0.7$ to make it possible to simultaneously cover the Hβ and the MgIIλ2800 line. The flux limit ensures that the S/N is high enough for a reliable analysis of the Hβ and MgIIλ2800 profiles that are contaminated, especially by extended FeII emission [69,70]. The sample is large enough to ensure that all spectral bins identified in Figure 1 are sufficiently populated. In addition, even if MgIIλ2800 lines are known to be narrower than Hβ in Population B [42,71–73], suggesting a larger emissivity-weighted distance from the continuum source for the MgIIλ2800 line [74–76], Hβ and MgIIλ2800 are both low-ionization lines expected to be predominantly emitted in a low-ionization, virialized part of the BLR [52,77,78] and to therefore show consistent profiles.

Our selection criterion is based on the presence of peculiarities in the emission line profiles. The correlations along the main sequence MS provide a robust framework to identify what is peculiar or, at the very least, rare. For example, the prominent red wing observed in the Hβ profile is a characteristic feature encompassing most of Population B, which constitutes approximately half of optically selected quasar samples [35,79]. While the origin of this feature remains unclear, it is not considered a peculiarity. In contrast, double- or multi-peaked profiles, as well as strongly shifted emission lines, are rare. A systematic line profile analysis along the MS reveals that they tend to be concentrated among quasars with the broadest Hβ profiles [37]. These cases also frequently exhibit rapid profile variability, occasionally leading to the "changing look" phenomenon [80,81]. In Population A, large inter-line shifts are easily understood in the framework of a system accretion disk + wind [52].

Seventeen sources belong to the spectral type B1^{++}, about 2.5% of the full sample. Their identification is reported in Table 1, along with the SDSS redshift, radio classification, qualitative Hβ profile classification following Sulentic [82], centroid shift at 0.9 fractional intensity. Measurements were obtained through non-linear, multi-components fits of the SDSS spectra within `IRAF v.2.18` [83–85], using the task `specfit` [86]. The same multi-component decomposition has an heuristic base and has been applied in tens of works in the past 25 years [78]. For a previous application on median spectra of the same sample considered here, see Marziani et al. [42].

The classification of Sulentic [82] assigns an asymmetry code to the broad-line profile (asymmetric to the red (AR) or to the blue (AB), or symmetric) and a code for the line peak shift (R or B). The centroids at different fractional intensities are as originally defined by Marziani et al. [52] and applied in several more recent works (for example, [87]).

Table 1. Basic properties of the B1^{++} sample.

Identification (1)	**Jcode** (2)	$z_{\rm SDSS}$ (3)	**Radio** (4)	**Hβ** (5)	$c(0.9)$ **Hβ** (6)	**Bin.?** (7)
WISEA J093642.95+551119.2	J093642	0.4971	RQ	AR,R	1309	Y
SDSS J101230.78+182021.1	J101230	0.4623	RL	AR,B	−480	Y
FBQS J110001.0+231412	J110001	0.5567	RL	AR,R	490	–
3C 254	J111438	0.7359	RL	AR,R	2225	Y
FBQS J111903.2+385852	J111903	0.7344	RL	AR,B	−2149	Y
HB89 1156+631	J115839	0.5924	RQ	AR,B	−349	Y
PG 1201+436	J120424	0.6617	RQ	AR,B	−1374	Y [a]
FBQS J1300+2830	J130028	0.6467	RL	AB,R	1781	Y
WISEA J130704.39+091004.1	J130704	0.5247	RQ	AR,B	3086 [b]	Y
SDSS J133051.90+184932.9	J133051	0.5141	RL	AR,B	−885	Y
WISE J133655.49+654115.9	J133655	0.4378	RQ	AR,R	172	Y [a]
FBQS J140012.6+353930	J140012	0.5184	RQ	AR,R	2341	Y
WISEA J141312.59+564113.3	J141312	0.6686	RL	AR,0	53	—
WISEA J150249.02+081305.9	J150249	0.5186	RQ	AR,B	7	Y
FBQS J153159.1+242047	J153159	0.6321	RL	AR,R	597	—
WISEA J155330.23+223010.3	J155330	0.6404	RQ	AR,B	−1809	Y
WISEA J163206.04+441659.5	J163206	0.5304	RQ	AB,B	−411	Y

Notes: Col. (1): common name recognizable by the NASA extragalactic database (NED); (2) code in the form Jhhmmss; (3) redshift reported in the header of the original SDSS spectra; (4) radio classification following Zamfir et al. [88]; (5) Hβ profile classification following Sulentic [82]. 0 means peak shift consistent with rest frame within the uncertainties; (6) centroid at 0.9 fractional intensity of Hβ, in km s^{-1}; (7) answer to the question, is the target a potential SMBBH candidate? [a]: boxy, [b]: peak shifted to the blue $v \sim -3550$ km s^{-1}.

4. Results

The benchmark classification for non-peculiar sources in Population B is AR,R or AR,0, where peak shifts at peak are usually modest, $\lesssim$ a few hundreds km s^{-1} [35,69,89]. Large shifts ($\gtrsim$1000 km s^{-1}) are rare and should be considered peculiar. Table 1 reports the amplitude of the centroid at 0.9 fractional intensity $c(0.9)$ that is considered a proxy of the line peak shift. Only three sources in Table 1 show an Hβ profile consistent with the reference AR,R profile for Population B. All the remaining sources show some peculiarities, with eight sources showing large shifts with absolute amplitude $\gtrsim$1000 km s^{-1}, suggesting that the origin of the perturbation is located in correspondence of the BLR. In one case (J130704), the actual peak is even displaced to the blue while the $c(0.9)$ is shifted to the red. This case highlights the large prevalence pf discordant asymmetries and peak shifts.

Figure 2 shows three cases, two of which depict the profiles of a binary system with a perturber with different, extreme projections of its velocity along the line of sight. The profile of MgIIλ2800 is narrower and more symmetric, as found in previous studies [71,72,74] and is shown in the third column of Figure 2. The classifications reported in Table 1 suggest that most sources have a peak shift that might be associated with excess emission over an AR profile. This is confirmed by the distribution of centroids for Hβ and MgIIλ2800. Figure 3 shows the distribution of the centroids at $\frac{1}{4}$, $\frac{1}{2}$, $\frac{3}{4}$ and 0.9 fractional intensity. The $c(0.9)$ of Hβ (bottom rightmost panel of Figure 3) shows a uniform distribution over a range ~-2000–$+3000$ km s^{-1}. A consistent distribution is also observed for $c(\frac{3}{4})$. At a lower fractional intensity, the shifts to the red associated with the prominent Hβ red wing typical of Population B dominates. In other words, apart from a few cases, the impression is the one of a perturbation affecting the top of the profile.

Figures 2 and 3 suggest two possibilities. The first is that the profile is affected by an outflow. The second is that there is a perturbation yielding a shifted peak. In the case of B1^{++} the outflow cannot be ruled out, but it is not favored by the large shift of the profiles. An outflow component is present in the Hβ profile of Pop. B; however, it is typically associated with the semi-broad component of [OIII]$\lambda\lambda$4959,5007 [90] and with shifts of a few hundred km s^{-1}. The centroid at $\frac{3}{4}$ measurements are available only for the sample of Zamfir et al. [79]. Out of 169 B1 sources, only 3 show $|c(\frac{3}{4})| \gtrsim 1000$ km s^{-1}. The distribution of B1 is much more centrally concentrated with a modest dispersion (gray box in Figure 3). A Kolmogorov–Sminrnov test carried out on the 169 B1 and on the 13 B1^{++} confirms that the two distributions are significantly different at a confidence level $\gtrsim 4\sigma$.

Prominent outflows affecting the profiles up to $\gtrsim$1000 km s^{-1} are seen only in Population A and extreme Population A at the opposite end of the sequence, where the ratio of radiative to gravitational forces is highest [62,63,91].

The interpretation of the red wing is not fully clear. However, the consensus is that it is a $M_{\rm BH}$ effect, either because of infall [55] or because of gravitational and transverse redshift [54,58,92–95]. The very broad, red wing becomes more prominent for very massive black holes powering the most luminous quasars [56,89], supporting the idea that the Hβ line profile is mostly broadened in the velocity field of a very massive black hole (as in extreme Population B). Figure 4 presents the luminosity-to-mass diagram for a sample of type-1 AGN, with the distribution of quasars from the considered sample overlaid for comparison. The data points cluster in correspondence of a fairly well-defined limit in Eddington ratio [35], below which the black holes are expected to enter in an inefficient radiative domain (e.g., [96–99]). They involve very massive sources, if black hole mass is estimated using standard relations [100]. This property is consistent with the prominent redward asymmetry and large shifts to the red toward the Hβ line base that are observed in the B1^{++} sample, if these are due to gravitational and transverse redshift. The main body of the line profiles is attributed to the velocity field of virialized gas within the gravitational field of a supermassive black hole, with gravitational redshift becoming increasingly significant as the emitting gas approaches the center of gravity. In contrast, the peaks of the profiles appear to be influenced by perturbations that account for only a small fraction of the line flux. The last column of Table 1 identifies the profiles that can be interpreted along this framework, i.e., the sources that could be considered candidates for eventual monitoring.

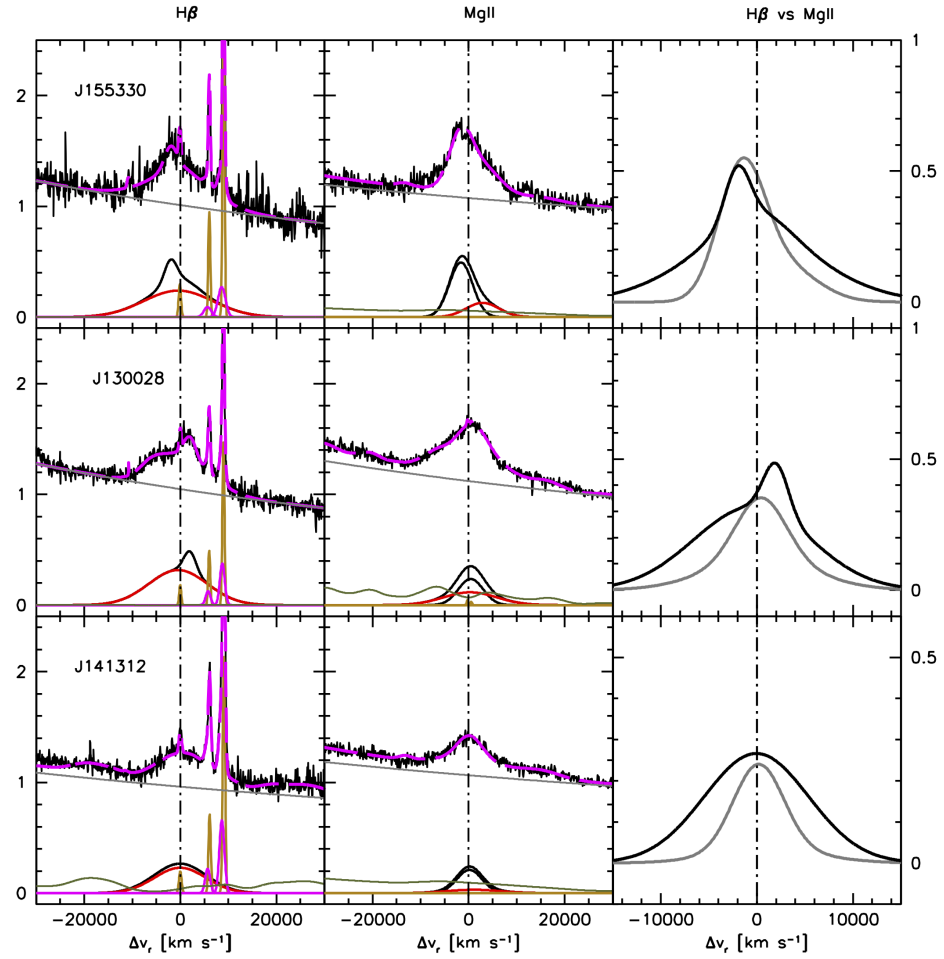


Figure 2. Examples of emission line profile analysis for Hβ (left column) and MgIIλ2800 (middle column). The top plot of each panel shows the original spectrum (thin black line) and the full model (dashed magenta line) along with the adopted continuum (gray). The bottom plots show the multiple components employed in the non-linear fit as follows: broad and very broad Hβ component (black and red Gaussians) [101,102], Hβ and [OIII]$\lambda\lambda$4959,5007 narrow line emission (gold), semi-broad emission of [OIII]$\lambda\lambda$4959,5007 (magenta) and FeII (dark green). FeII emission is very weak in most of the sample, both in the optical and in the UV. The right column shows a comparison between the Hβ and MgIIλ2800 (gray) broad profiles.

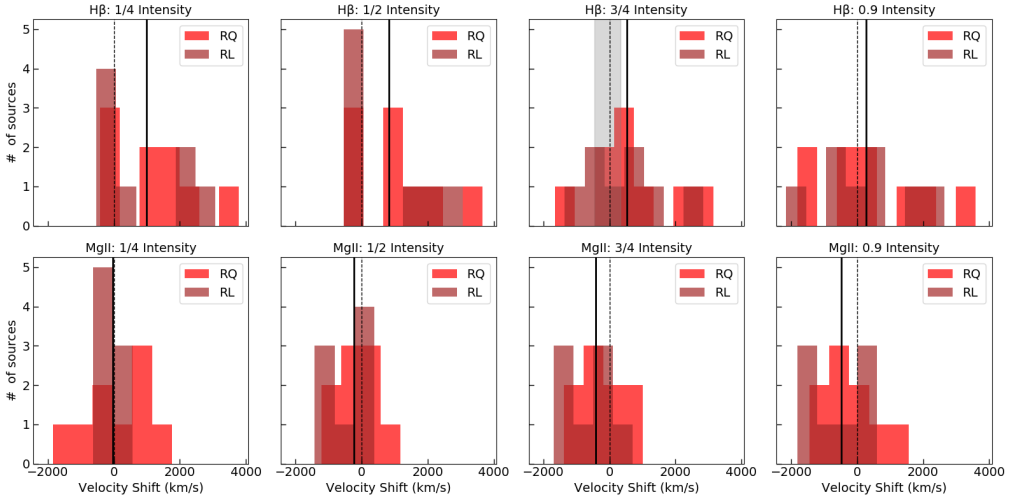


Figure 3. Distribution of centroids at four different fractional intensity levels, from left to right $\frac{1}{4}$, $\frac{1}{2}$, $\frac{3}{4}$ and 0.9. **Top**: Hβ; **bottom**: MgIIλ2800. Radio-loud sources are shaded brown. The rest frame radial

velocity is represented by the dashed line, while the thick black line is the average of the sample. The shaded gray box shows the $\pm 1\sigma$ range for the $c(\frac{3}{4})$ measurement of the B1 spectral type from the sample of Zamfir et al. [79].

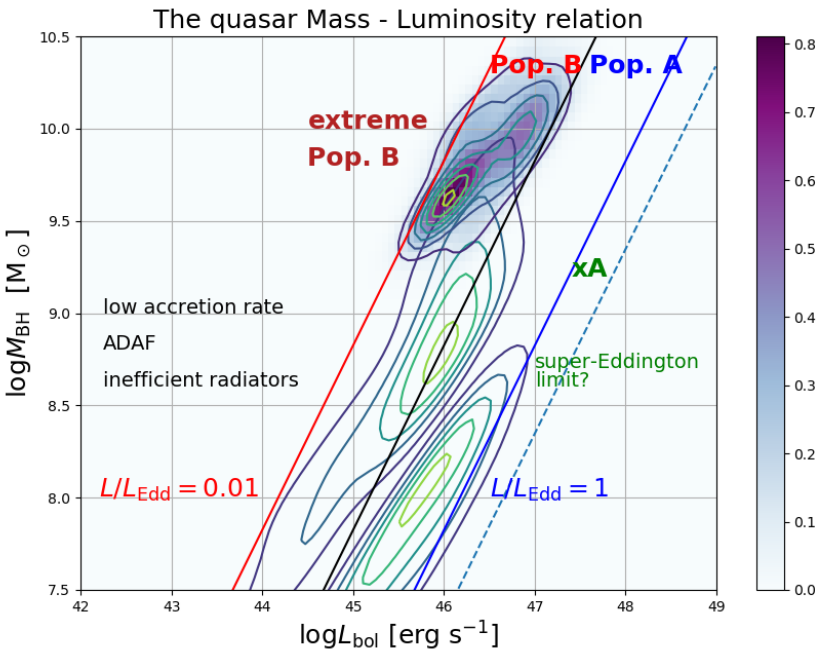


Figure 4. The black hole mass–luminosity diagram for a low-z type quasar sample. The B1^{++} quasar location in the $M_{\rm BH}$– L diagram corresponds to the contour in the middle upper part of the diagram. The vast majority are located close to the limit $L/L_{\rm Edd} \sim 10^{-2}$, close to the domain expected for inefficient radiators. The black diagonal line at $L/L_{\rm Edd} = 0.1$ separates Population A and B. On the high Eddington ratio side, the possible super-Eddington accretors are labeled as xA (extreme Population A), with Eddington ratios not exceeding 1 by a large factor, as found observationally [103], and as derived from the theory of super-Eddington accretion disks as well [104–107].

5. Discussion

5.1. A SMBBH System

The simplest interpretation in terms of a SMBBH system is of a very massive primary (leading to the Hβ profile with redshift increasing toward the line base) with a secondary of small mass ratio $q \sim 0.1$, capable of inducing a measurable effect on the BLR region velocity field and accretion disk, and even jet precession (e.g., [108,109]). There are several factors that may increase the detectability of SMBBHs in the spectral type B1^{++}. The first one is due to orientation. The current interpretation of the BLR of Pop. B is the one of a highly flattened system, coplanar with the accretion disk [90,110,111]. The extreme line width, and the high prevalence of radio sources whose radio axis is seen at a large angle [65,112,113], indicates that the velocity field projection along the line of sight is maximized for B1^{++} sources. B1^{++} can be connected to blazars (sources of low Eddington ratio and minimal FeII emission [114] by an exclusive orientation effect, as blazars are oriented with the jet closely aligned to the line-of-sight (Figure 3 by Marziani et al. [115]), but are otherwise believed to be low accretors. However, orientation alone cannot explain the properties of the B1^{++}.

The low FeII emission and the extreme broad line width with pronounced redward asymmetries point toward extremely high $M_{\rm BH}$ and extremely low $L/L_{\rm Edd}$. Indeed, the B1^{++} sources show similar $M_{\rm BH} \sim 10^{10}$ solar masses and moderate luminosity due to low Eddington ratio $\sim 10^{-2}$. In other words, they are evolved system close to (but not yet in) the condition of "spent" quasars [116]. The presence of a second black hole with $q \gtrsim 0.04$ may

induce a truncation in the BLR emission, as the mass flow in the circum-binary Keplerian disk is perturbed by tidal forces which carve annular gaps in the second black hole orbital path [117,118], hampering to various extent the accretion process [119]. This might be the case of the classical double "peakers" with a broad-line profile consistent with the emission from an accretion disk truncated at ∼1000 gravitational radii [120–123].

The average optical luminosity of the B1^{++} quasars, $\sim 5 \cdot 10^{45}$ erg s^{-1}, implies a BLR radius $\sim 5 \cdot 10^{17}$cm $\lesssim$ 1 pc, identifying these systems as bona-fide sub-parsec binary candidates. The time to coalescence because of gravitational wave emission is provided by the relation $T_c = \frac{15}{304} \frac{c^5 a_0^4}{G^3 M_1 M_2 (M_1+M_2)} \cdot (1-e_0^2)^{7/2} \cdot \frac{1}{g(e_0)}$, where $g(e_0) = 1 + \frac{73}{24} e_0^2 + \frac{37}{96} e_0^4$ [124,125], where e_0 is the initial eccentricity. In our case, assuming that $M_2 = 0.1 M_1$, with $M_1 = 10^{10}$ solar masses, we obtain a coalescence time $\sim 10^7$ yr for a circular orbit for $e_0 = 0$. The T_c can be significantly shortened only if the eccentricity is rather high as follows: by a factor 10 if $e_0 = 0.6$, and by a factor 100 if $e_0 = 0.8$. With an orbital period $P \gtrsim 10^2$ yr, the immediate prediction is that the peculiar, displaced peaks should not show any short term variation ($\lesssim$1 yr), while a systematic shift over 10–20 yr might occur. At the very least, the B1^{++} spectral type can be considered an appropriate testbed for the SMBBH model (see also [126]).

The inspiral motion of a less massive black hole in the gravitational field of a supermassive black hole produces a distinctive gravitational wave signal characterized by long-duration, low-frequency waveforms. These signals result from the gradual inspiral of a compact object toward the SMBH. For the sample considered in this study, the black hole masses are extremely large and inspiral motions may produces waves of frequencies in the domain of the Pulsar Timing Array ([127,128], $\nu \sim 10^{-9}$).

5.2. The Latest Phases of Evolution Along the Quasar Main Sequence

We might expect a rich phenomenology in the frequency domains covered by planned space- and ground-based detectors due to the remnants of a nuclear stellar system [129]. Nuclear (i.e., within the molecular torus) and circumnuclear star formation occurs in most AGN with moderate or high accretion rates [130–133]. The outer self-gravitating disk and torus provide gas for nuclear fueling, with star formation naturally associated with high or super-Eddington accretion [134–140]. As quasars evolve, feedback processes deplete surrounding material, leading to lower $L/L_{\rm Edd}$ ratios and a transition into Population B, characterized by weaker outflows and stronger core [OIII]$\lambda\lambda$4959,5007 emission [37]. Fraix-Burnet et al. [141] list several multi-frequency parameters that are systematically different between Population A and B. Extreme Population B sources can be thought as simply reaching the most extreme values in most observational parameters of Population B. The torus may be absent in such low-luminosity AGN [142], leaving the black hole without a large reservoir of accreting matter. The point here is what may happen in the nuclear regions of such an evolved stellar system.

The fate of such a system remains unclear. The best prospect for detecting it lies in gravitational radiation, since the electromagnetic signal is overwhelmed by the luminosity of the AGN. The scenario envisaged for super-Eddington accretors will ultimately lead to a population of stellar mass compact objects, and to intermediate mass black holes (IMBHs) [135,143–146].

5.3. GW from IMBH and Stellar Mass Black Hole Coalescence

Observed nuclear star clusters have extremely high stellar density, exceeding 10^6 $M_\odot$ [147,148], and runaway collisions of massive stars [143,144] could be a pathway to generate IMBHs of 10^4–10^5 $M_\odot$. A second pathway is via the enhancement of stellar black hole merger rates in the dense environment of the accretion disk due to the increased

probability of BH–BH encounters, binary formation via orbital migration and migration traps [149]. An IMBH could in turn become a seed black hole in a binary system, and lead to an extreme mass ratio inspiral (EMRI) phenomenology. The gravitational wave frequencies from EMRIs typically fall in the millihertz range, which makes them ideal targets for future space-based gravitational wave detectors like the Laser Interferometer Space Antenna (LISA, [7,8]). LISA will be sensitive to the low-frequency gravitational waves emitted by EMRIs with primary masses covering the domain of IMBHs up to moderately SMBBH ($\sim 10^8$ $M_\odot$, [7,150]), which cannot be detected by ground-based observatories due to their low frequency range.

The first IMBH gravitational-wave detections, such as GW150914, involved black holes of about 29 and 36 solar masses [151], which are thought to be formed by the direct collapse of massive stars in low-metallicity environments [152,153]. If the progenitor of the remnant black holes were high metallicity stars, it might be that the initial mass after collapse could be as large as 30 $M_\odot$ [154,155]. In AGN disks, stellar-mass black hole mergers are expected to occur at a higher rate than in isolated environments [156] and produce gravitational wave bursts [157]. The high frequency of mergers is expected, in turn, to produce a post-AGN population of $\sim$10 $M_\odot$ black holes [158], along with a population of IMBHs [146,158].

The signal amplitude of gravitational waves from a binary BH merger is typically expressed in terms of the strain amplitude h, which depends on the masses of the black holes, the distance to the merger, and the orientation of the system relative to the observer. For a stellar-mass black hole merger, let us assume both black holes have masses of $5M_\odot$, typical of a general population of remnant black holes [159]. The chirp mass is $M_c = \frac{(M_1 M_2)^{3/5}}{(M_1+M_2)^{1/5}} \approx 4.35 M_\odot$. The GW strain amplitude h for a circular binary inspiral of two masses M_1 and M_2 is approximated by $h \approx \frac{4(GM_c)^{5/3}}{c^4 D_L}(\pi f)^{2/3}$, where G is the gravitational constant, f is the gravitational wave frequency, D_L is the luminosity distance to the source, and c is the speed of light. Frequencies in the range from 10 Hz to 1000 Hz are typically considered in a binary black hole inspiral. Ground-based interferometers like the Laser Interferometer Gravitational-Wave Observatory (LIGO [160]) and Virgo [161] are optimized for detecting the mergers of stellar-mass black holes. A frequency $f = 100$ Hz is in the sensitivity range for both LIGO and the Einstein Telescope (ET, [162,163]). The strain h for a merger at $z \approx 0.55$ is $h \sim 10^{-23}$. The strain sensitivity of LIGO's O3 run is about $h \sim 10^{-23}$ to 10^{-24} at its peak sensitivity. This means that LIGO detects BBH mergers up to typical redshift of the B1^{++} sample. The ET will be 10 to 100 times more sensitive than LIGO, extending the detection horizon to much higher redshifts. The ET will be capable of detecting strain amplitudes as low as $h \sim 10^{-25}$, or even smaller, and comfortably sample the stellar-mass BH remnant population expected in evolved AGN.

6. Conclusions

This study has highlighted the potential of the quasar main sequence as a framework to identify promising candidates for supermassive binary black holes (SMBBHs). By focusing on a specific spectral type along the quasar main sequence, B1^{++}, we identified emission line peculiarities, such as large centroid shifts, which may indicate the presence of secondary compact objects perturbing the accretion dynamics. These findings suggest that high-mass black holes with low Eddington ratios, typical of B1^{++} sources, are favorable environments for detecting SMBBHs.

Future multi-wavelength campaigns and gravitational wave observations are essential for confirming these systems. Sub-parsec binaries within this spectral class may also provide crucial insights into the role of tidal forces and binary-induced disk perturbations in shaping AGN emission profiles and evolutionary pathways.

Author Contributions: Writing—original draft preparation, P.M.; Conceptualization, reading, and correction of the draft, E.B., N.B. and M.D. All authors have read and agreed to the published version of the manuscript.

Funding: This research was funded by Ministry of Science, Technological Development and Innovation of the Republic of Serbia, grant number 451-03-136/2025-03/200002.

Data Availability Statement: This paper is based entirely on published data (SDSS). A table of measurement has been uploaded along with the paper.

Acknowledgments: E.B. and N.B. acknowledge the support of the Ministry of Science, Technological Development and Innovation of the Republic of Serbia. Funding for the SDSS and SDSS-II has been provided by the Alfred P. Sloan Foundation, the Participating Institutions, the National Science Foundation, the U.S. Department of Energy, the National Aeronautics and Space Administration, the Japanese Monbukagakusho, the Max Planck Society, and the Higher Education Funding Council for England. The present-day SDSS website is http://classic.sdss.org/dr7/ (originally accessed on 1 July 2012). The SDSS is managed by the Astrophysical Research Consortium for the participating institutions. The participating institutions are the American Museum of Natural History, Astrophysical Institute Potsdam, University of Basel, University of Cambridge, Case Western Reserve University, University of Chicago, Drexel University, Fermilab, the Institute for Advanced Study, the Japan Participation Group, Johns Hopkins University, the Joint Institute for Nuclear Astrophysics, the Kavli Institute for Particle Astrophysics and Cosmology, the Korean Scientist Group, the Chinese Academy of Sciences (LAMOST), Los Alamos National Laboratory, the Max–Planck–Institute for Astronomy (MPIA), the Max–Planck–Institute for Astrophysics (MPA), New Mexico State University, Ohio State University, University of Pittsburgh, University of Portsmouth, Princeton University, the United States Naval Observatory, and the University of Washington.

Conflicts of Interest: The authors declare no conflicts of interest.

Abbreviations

The following abbreviations are used in this manuscript:

AGN	Active Galactic Nucleus/i
BH	Black Hole
BLR	Broad Line Region
E1	Eigenvector 1
ET	Einstein Telescope
EMRI	Extreme Mass Ratio Inspiral
FWHM	Full Width Half Maximum
GW	Gravitational Wave
LIGO	Laser Interferometer Gravitational-Wave Observatory
LISA	Laser Interferometer Space Antenna
LIL	Low Ionization Line
MDPI	Multidisciplinary Digital Publishing Institute
MS	Main Sequence
NLSy1	Narrow Line Seyfert 1
PCA	Principal Component Analysis
PTF	Palomar Transient Factory
RL	Radio-Loud
RQ	Radio-Quiet
SDSS	Sloan Digital Sky Survey
SMBH	Supermassive Black Hole
SMBBH	Supermassive Binary Black Hole
xA	extreme (Population) A
ZTF	Zwicky Transient Facility

References

1. Colpi, M. Massive Binary Black Holes in Galactic Nuclei and Their Path to Coalescence. *Space Sci. Rev.* **2014**, *183*, 189–221. [CrossRef]
2. Komossa, S.; Ciprini, S.; Dey, L.; Gallo, L.C.; Gomez, J.L.; Gonzalez, A.; Grupe, D.; Kraus, A.; Laine, S.J.; Parker, M.L.; et al. Supermassive Binary Black Holes and the Case of OJ 287. In Proceedings of the XIX Serbian Astronomical Conference, Belgrade, Serbia, 13–17October 2020; Publications of the Astronomical Observatory of Belgrade; Kovačević, A., Kovačević Dojčinović, J., Marčeta, D., Onić, D., Eds.; Volume 100, pp. 29–42. [CrossRef]
3. Komossa, S.; Grupe, D. The Extremes of Continuum and Emission-Line Variability of AGN: Changing-Look Events and Binary SMBHS. *Serbian Astron. J.* **2024**, *209*, 1–24. [CrossRef]
4. Burke-Spolaor, S.; Bailes, M.; Johnston, S.; Bates, S.D.; Bhat, N.D.R.; Burgay, M.; D'Amico, N.; Jameson, A.; Keith, M.J.; Kramer, M.; et al. The High Time Resolution Universe Pulsar Survey—III. Single-pulse searches and preliminary analysis. *Mon. Not. R. Astron. Soc.* **2011**, *416*, 2465–2476. [CrossRef]
5. Theureau, G.; Babak, S.; Berthereau, A.; Chalumeau, A.; Chen, S.; Cognard, I.; Falxa, M.; Guillemot, L.; Petiteau, A. Pulsar Timing Arrays and gravitational waves: The first steps towards detection? In Proceedings of the SF2A-2021: Proceedings of the Annual Meeting of the French Society of Astronomy and Astrophysics, Online, 7–11 June 2021; Siebert, A., Baillié, K., Lagadec, E., Lagarde, N., Malzac, J., Marquette, J.B., N'Diaye, M., Richard, J., Venot, O., Eds.; pp. 23–28.
6. Berti, E.; Cardoso, V.; Will, C.M. Gravitational-wave spectroscopy of massive black holes with the space interferometer LISA. *Phys. Rev. D* **2006**, *73*, 064030. [CrossRef]
7. Amaro-Seoane, P.; Audley, H.; Babak, S.; Baker, J.; Barausse, E.; Bender, P.; Berti, E.; Binetruy, P.; Born, M.; Bortoluzzi, D.; et al. Laser Interferometer Space Antenna. *arXiv* **2017**, arXiv:1702.00786. [CrossRef]
8. D'Onofrio, M.; Marziani, P. A multimessenger view of galaxies and quasars from now to mid-century. *Front. Astron. Space Sci.* **2018**, *5*, 31. [CrossRef]
9. Sillanpaa, A.; Haarala, S.; Valtonen, M.J.; Sundelius, B.; Byrd, G.G. OJ 287-Binary pair of supermassive black holes. *Astrophys. J.* **1988**, *325*, 628–634. [CrossRef]
10. Valtonen, M.J.; Lehto, H.J.; Nilsson, K.; Heidt, J.; Takalo, L.O.; Sillanpää, A.; Villforth, C.; Kidger, M.; Poyner, G.; Pursimo, T.; et al. A massive binary black-hole system in OJ 287 and a test of general relativity. *Nature* **2008**, *452*, 851–853. [CrossRef]
11. Valtonen, M.J.; Dey, L.; Gopakumar, A.; Zola, S.; Lähteenmäki, A.; Tornikoski, M.; Gupta, A.C.; Pursimo, T.; Knudstrup, E.; Gomez, J.L.; et al. Observational Implications of OJ 287's Predicted 2022 Disk Impact in the Black Hole Binary Model. *Galaxies* **2023**, *11*, 82. [CrossRef]
12. Eracleous, M.; Halpern, J.P.; Gilbert, A.M.; Newman, J.A.; Filippenko, A.V. Rejection of the Binary Broad-Line Region Interpretation of Double-peaked Emission Lines in Three Active Galactic Nuclei. *Astrophys. J.* **1997**, *490*, 216. [CrossRef]
13. Gezari, S.; Halpern, J.P.; Eracleous, M. Long-Term Profile Variability of Double-peaked Emission Lines in Active Galactic Nuclei. *Astrophys. J. Suppl.* **2007**, *169*, 167–212. [CrossRef]
14. Liu, T.; Gezari, S.; Miller, M.C. Did ASAS-SN Kill the Supermassive Black Hole Binary Candidate PG1302-102? *Astrophys. J. Lett.* **2018**, *859*, L12. [CrossRef]
15. Volonteri, M.; Haardt, F.; Madau, P. The Assembly and Merging History of Supermassive Black Holes in Hierarchical Models of Galaxy Formation. *Astrophys. J.* **2003**, *582*, 559–573. [CrossRef]
16. Volonteri, M.; Miller, J.M.; Dotti, M. Sub-Parsec Supermassive Binary Quasars: Expectations at $z < 1$. *Astrophys. J. Lett.* **2009**, *703*, L86–L89. [CrossRef]
17. Merritt, D.; Milosavljević, M. Massive black hole binary evolution in stellar environments: Implications for gravitational wave detection. *Living Rev. Relativ.* **2005**, *8*, 8. [CrossRef]
18. Graham, M.J.; Djorgovski, S.G.; Stern, D.; Drake, A.J.; Mahabal, A.A.; Donalek, C.; Glikman, E.; Larson, S.; Christensen, E. A systematic search for close supermassive black hole binaries in the Catalina Real-time Transient Survey. *Mon. Not. R. Astron. Soc.* **2015**, *453*, 1562–1576. [CrossRef]
19. Chambers, K.C.; Magnier, E.A.; Metcalfe, N.; Flewelling, H.A.; Huber, M.E.; Waters, C.Z.; Denneau, L.; Draper, P.W.; Farrow, D.; Finkbeiner, D.P.; et al. The Pan-STARRS1 Surveys. *arXiv* **2016**, arXiv:1612.05560. [CrossRef]
20. Bellm, E.C.; Kulkarni, S.R.; Graham, M.J.; Dekany, R.; Smith, R.M.; Riddle, R.; Masci, F.J.; Helou, G.; Prince, T.A.; Adams, S.M.; et al. The Zwicky Transient Facility: System Overview, Performance, and First Results. *Publ. Astron. Soc. Pac.* **2019**, *131*, 018002. [CrossRef]
21. Graham, M.J.; Kulkarni, S.R.; Bellm, E.C.; Adams, S.M.; Barbarino, C.; Blagorodnova, N.; Bodewits, D.; Bolin, B.; Brady, P.R.; Cenko, S.B.; et al. The Zwicky Transient Facility: Science Objectives. *Publ. Astron. Soc. Pac.* **2019**, *131*, 078001. [CrossRef]
22. Masci, F.J.; Laher, R.R.; Rusholme, B.; Shupe, D.L.; Groom, S.; Surace, J.; Jackson, E.; Monkewitz, S.; Beck, R.; Flynn, D.; et al. The Zwicky Transient Facility: Data Processing, Products, and Archive. *Publ. Astron. Soc. Pac.* **2019**, *131*, 018003. [CrossRef]

23. Charisi, M.; Bartos, I.; Haiman, Z.; Price-Whelan, A.M.; Graham, M.J.; Bellm, E.C.; Laher, R.R.; Márka, S. A population of short-period variable quasars from PTF as supermassive black hole binary candidates. *Mon. Not. R. Astron. Soc.* **2016**, *463*, 2145–2171. [CrossRef]
24. Vaughan, S.; Uttley, P.; Markowitz, A.G.; Huppenkothen, D.; Middleton, M.J.; Alston, W.N.; Scargle, J.D.; Farr, W.M. False periodicities in quasar time-domain surveys. *Mon. Not. R. Astron. Soc.* **2016**, *461*, 3145–3152. [CrossRef]
25. Edelman, A.; Liu, X. The role of red noise in false periodicity detection in AGN light curves. *Astrophys. J.* **2023**, *949*, 56. [CrossRef]
26. Horne, J.H.; Baliunas, S.L. A Prescription for Period Analysis of Unevenly Sampled Time Series. *Astrophys. J.* **1986**, *302*, 757. [CrossRef]
27. Sesar, B.; Ivezić, Ž.; Lupton, R.H.; Jurić, M.; Gunn, J.E.; Knapp, G.R.; DeLee, N.; Smith, J.A.; Miknaitis, G.; Lin, H.; et al. Exploring the Variable Sky with the Sloan Digital Sky Survey. *Astron. J.* **2007**, *134*, 2236–2251. [CrossRef]
28. Hilditch, R.W. *An Introduction to Close Binary Stars*; Cambridge University Press: Cambridge, UK, 2001.
29. Bon, E.; Jovanović, P.; Marziani, P.; Shapovalova, A.I.; Bon, N.; Borka Jovanović, V.; Borka, D.; Sulentic, J.; Popović, L.Č. The First Spectroscopically Resolved Sub-parsec Orbit of a Supermassive Binary Black Hole. *Astrophys. J.* **2012**, *759*, 118. [CrossRef]
30. Shen, Y.; Liu, X.; Loeb, A.; Tremaine, S. Constraining Sub-parsec Binary Supermassive Black Holes in Quasars with Multi-epoch Spectroscopy. I. The General Quasar Population. *Astrophys. J.* **2013**, *775*, 49. [CrossRef]
31. Li, Y.R.; Wang, J.M.; Ho, L.C.; Lu, K.X.; Qiu, J.; Du, P.; Hu, C.; Huang, Y.K.; Zhang, Z.X.; Wang, K.; et al. Spectroscopic Indication of a Centi-parsec Supermassive Black Hole Binary in the Galactic Center of NGC 5548. *Astrophys. J.* **2016**, *822*, 4. [CrossRef]
32. Robinson, A.; Young, S.; Axon, D.J.; Kharb, P.; Smith, J.E. Spectropolarimetric Evidence for a Kicked Supermassive Black Hole in the Quasar E1821+643. *Astrophys. J. Lett.* **2010**, *717*, L122–L126. [CrossRef]
33. Jadhav, Y.; Robinson, A.; Almeyda, T.; Curran, R.; Marconi, A. The spatially offset quasar E1821+643: New evidence for gravitational recoil. *Mon. Not. R. Astron. Soc.* **2021**, *507*, 484–495. [CrossRef]
34. Boroson, T.A.; Green, R.F. The Emission-Line Properties of Low-Redshift Quasi-stellar Objects. *Astrophys. J. Suppl.* **1992**, *80*, 109. [CrossRef]
35. Marziani, P.; Zamanov, R.K.; Sulentic, J.W.; Calvani, M. Searching for the physical drivers of eigenvector 1: Influence of black hole mass and Eddington ratio. *Mon. Not. R. Astron. Soc.* **2003**, *345*, 1133–1144. [CrossRef]
36. Shen, Y.; Ho, L.C. The diversity of quasars unified by accretion and orientation. *Nature* **2014**, *513*, 210–213. [CrossRef] [PubMed]
37. Sulentic, J.W.; Marziani, P.; Dultzin-Hacyan, D. Phenomenology of Broad Emission Lines in Active Galactic Nuclei. *Annu. Rev. Astron. Astrophys.* **2000**, *38*, 521–571. [CrossRef]
38. Sulentic, J.W.; Marziani, P.; Zwitter, T.; Dultzin-Hacyan, D.; Calvani, M. The Demise of the Classical Broad-Line Region in the Luminous Quasar PG 1416-129. *Astrophys. J. Lett.* **2000**, *545*, L15–L18. [CrossRef]
39. Panda, S.; Marziani, P.; Czerny, B. The Quasar Main Sequence Explained by the Combination of Eddington Ratio, Metallicity, and Orientation. *Astrophys. J.* **2019**, *882*, 79. [CrossRef]
40. Jankov, I.; Ilić, D.; Kovačević, A. Manifold Learning in the Context of Quasar Spectral Diversity. In Proceedings of the XIX Serbian Astronomical Conference, Belgrade, Serbia, 13–17 October 2020; Kovačević, A., Kovačević Dojčinović, J., Marčeta, D., Onić, D., Eds.; Volume 100, pp. 241–246.
41. Ghojogh, B.; Ghodsi, A.; Karray, F.; Crowley, M. Locally Linear Embedding and its Variants: Tutorial and Survey. *arXiv* **2020**, arXiv:2011.10925. [CrossRef]
42. Marziani, P.; Sulentic, J.W.; Plauchu-Frayn, I.; del Olmo, A. Is Mg II 2800 a Reliable Virial Broadening Estimator for Quasars? *Astron. Astrophys.* **2013**, *555*, 89. [CrossRef]
43. Marinello, A.O.M.; Rodriguez-Ardila, A.; Garcia-Rissmann, A.; Sigut, T.A.A.; Pradhan, A.K. The FeII emission in active galactic nuclei: Excitation mechanisms and location of the emitting region. *Astrophys. J.* **2016**, *820*, 116. [CrossRef]
44. Marziani, P.; Sulentic, J.W.; Zwitter, T.; Dultzin-Hacyan, D.; Calvani, M. Searching for the Physical Drivers of the Eigenvector 1 Correlation Space. *Astrophys. J.* **2001**, *558*, 553–560. [CrossRef]
45. Sun, J.; Shen, Y. Dissecting the Quasar Main Sequence: Insight from Host Galaxy Properties. *Astrophys. J. Lett.* **2015**, *804*, L15. [CrossRef]
46. Du, P.; Wang, J.M.; Hu, C.; Ho, L.C.; Li, Y.R.; Bai, J.M. The Fundamental Plane of the Broad-line Region in Active Galactic Nuclei. *Astrophys. J. Lett.* **2016**, *818*, L14. [CrossRef]
47. Antonucci, R. Unified models for active galactic nuclei and quasars. *Annu. Rev. Astron. Astrophys.* **1993**, *31*, 473–521. [CrossRef]
48. Urry, C.M.; Padovani, P. Unified Schemes for Radio-Loud Active Galactic Nuclei. *Publ. Astron. Soc. Pac.* **1995**, *107*, 803. [CrossRef]
49. Marin, F.; Antonucci, R. A Robust Derivation of the Tight Relationship of Radio Core Dominance to Inclination Angle in High Redshift 3CRR Sources. *Astrophys. J.* **2016**, *830*, 82. [CrossRef]
50. Bon, N.; Marziani, P.; Bon, E.; Negrete, C.A.; Dultzin, D.; del Olmo, A.; D'Onofrio, M.; Martínez-Aldama, M.L. Selection of highly-accreting quasars. Spectral properties of Fe II$_{opt}$ emitters not belonging to extreme Population A. *Astron. Astrophys.* **2020**, *635*, A151. [CrossRef]

51. Collin-Souffrin, S.; Dyson, J.E.; McDowell, J.C.; Perry, J.J. The environment of active galactic nuclei. I-A two-component broad emission line model. *Mon. Not. R. Astron. Soc.* **1988**, *232*, 539–550. [CrossRef]
52. Marziani, P.; Sulentic, J.W.; Dultzin-Hacyan, D.; Calvani, M.; Moles, M. Comparative Analysis of the High- and Low-Ionization Lines in the Broad-Line Region of Active Galactic Nuclei. *Astrophys. J. Suppl.* **1996**, *104*, 37. [CrossRef]
53. Elvis, M. A Structure for Quasars. *Astrophys. J.* **2000**, *545*, 63–76. [CrossRef]
54. Netzer, H. On the profiles of the broad lines in the spectra of QSOs and Seyfert galaxies. *Mon. Not. R. Astron. Soc.* **1977**, *181*, 89P–92P. [CrossRef]
55. Wang, J.M.; Du, P.; Brotherton, M.S.; Hu, C.; Songsheng, Y.Y.; Li, Y.R.; Shi, Y.; Zhang, Z.X. Tidally disrupted dusty clumps as the origin of broad emission lines in active galactic nuclei. *Nat. Astron.* **2017**, *1*, 775–783. [CrossRef]
56. Wolf, J.; Salvato, M.; Coffey, D.; Merloni, A.; Buchner, J.; Arcodia, R.; Baron, D.; Carrera, F.J.; Comparat, J.; Schneider, D.P.; et al. Exploring the diversity of Type 1 active galactic nuclei identified in SDSS-IV/SPIDERS. *Mon. Not. R. Astron. Soc.* **2020**, *492*, 3580–3601. [CrossRef]
57. Bao, D.W.; Brotherton, M.S.; Du, P.; McLane, J.N.; Zastrocky, T.E.; Olson, K.A.; Fang, F.N.; Zhai, S.; Huang, Z.P.; Wang, K.; et al. Monitoring AGNs with Hβ Asymmetry. III. Long-term Reverberation Mapping Results of 15 Palomar-Green Quasars. *Astrophys. J. Suppl.* **2022**, *262*, 14. [CrossRef]
58. Marziani, P. Accretion/Ejection Phenomena and Emission-Line Profile (A)symmetries in Type-1 Active Galactic Nuclei. *Symmetry* **2023**, *15*, 1859. [CrossRef]
59. Zastrocky, T.E.; Brotherton, M.S.; Du, P.; McLane, J.N.; Olson, K.A.; Dale, D.A.; Kobulnicky, H.A.; Maithil, J.; Nguyen, M.L.; Chick, W.T.; et al. Monitoring AGNs with Hβ Asymmetry. IV. First Reverberation Mapping Results of 14 Active Galactic Nuclei. *Astrophys. J. Suppl.* **2024**, *272*, 29. [CrossRef]
60. Punsly, B.; Marziani, P.; Bennert, V.N.; Nagai, H.; Gurwell, M.A. Revealing the Broad Line Region of NGC 1275: The Relationship to Jet Power. *Astrophys. J.* **2018**, *869*, 143. [CrossRef]
61. Panda, S.; Czerny, B.; Adhikari, T.P.; Hryniewicz, K.; Wildy, C.; Kuraszkiewicz, J.; Śniegowska, M. Modeling of the Quasar Main Sequence in the Optical Plane. *Astrophys. J.* **2018**, *866*, 115. [CrossRef]
62. Sulentic, J.W.; Bachev, R.; Marziani, P.; Negrete, C.A.; Dultzin, D. C IV λ1549 as an Eigenvector 1 Parameter for Active Galactic Nuclei. *Astrophys. J.* **2007**, *666*, 757–777. [CrossRef]
63. Richards, G.T.; Kruczek, N.E.; Gallagher, S.C.; Hall, P.B.; Hewett, P.C.; Leighly, K.M.; Deo, R.P.; Kratzer, R.M.; Shen, Y. Unification of Luminous Type 1 Quasars through C IV Emission. *Astron. J.* **2011**, *141*, 167. [CrossRef]
64. Bonzini, M.; Mainieri, V.; Padovani, P.; Andreani, P.; Berta, S.; Bethermin, M.; Lutz, D.; Rodighiero, G.; Rosario, D.; Tozzi, P.; et al. Star formation properties of sub-mJy radio sources. *Mon. Not. R. Astron. Soc.* **2015**, *453*, 1079–1094. [CrossRef]
65. Ganci, V.; Marziani, P.; D'Onofrio, M.; del Olmo, A.; Bon, E.; Bon, N.; Negrete, C.A. Radio loudness along the quasar main sequence. *Astron. Astrophys.* **2019**, *630*, A110. [CrossRef]
66. Panessa, F.; Baldi, R.D.; Laor, A.; Padovani, P.; Behar, E.; McHardy, I. The origin of radio emission from radio-quiet active galactic nuclei. *Nat. Astron.* **2019**, *3*, 387–396. [CrossRef]
67. Chen, S.; Laor, A.; Behar, E.; Baldi, R.D.; Gelfand, J.D.; Kimball, A.E.; McHardy, I.M.; Orosz, G.; Paragi, Z. Windy or Not: Radio Parsec-scale Evidence for a Broad-line Region Wind in Radio-quiet Quasars. *Astrophys. J.* **2024**, *975*, 35. [CrossRef]
68. Marziani, P.; Sulentic, J.W.; Plauchu-Frayn, I.; del Olmo, A. Low-Ionization Outflows in High Eddington Ratio Quasars. *Astrophys. J.* **2013**, *764*, 150. [CrossRef]
69. Marziani, P.; Sulentic, J.W.; Zamanov, R.; Calvani, M.; Dultzin-Hacyan, D.; Bachev, R.; Zwitter, T. An Optical Spectroscopic Atlas of Low-Redshift Active Galactic Nuclei. *Astrophys. J. Suppl.* **2003**, *145*, 199–211. [CrossRef]
70. Kovačević-Dojčinović, J.; Popović, L.Č. The Connections Between the UV and Optical Fe ii Emission Lines in Type 1 AGNs. *Astrophys. J. Suppl.* **2015**, *221*, 35. [CrossRef]
71. Wang, J.; Dong, X.; Wang, T.; Ho, L.C.; Yuan, W.; Wang, H.; Zhang, K.; Zhang, S.; Zhou, H. Estimating Black Hole Masses in Active Galactic Nuclei Using the Mg II λ2800 Emission Line. *Astrophys. J.* **2009**, *707*, 1334–1346. [CrossRef]
72. Trakhtenbrot, B.; Netzer, H. Black hole growth to z = 2 - I. Improved virial methods for measuring M_{BH} and L/L_{Edd}. *Mon. Not. R. Astron. Soc.* **2012**, *427*, 3081–3102. [CrossRef]
73. Popović, L.Č.; Kovačević-Dojčinović, J.; Marčeta-Mandić, S. The structure of the Mg II broad line emitting region in Type 1 AGNs. *Mon. Not. R. Astron. Soc.* **2019**, *484*, 3180–3197. [CrossRef]
74. Shen, Y.; Horne, K.; Grier, C.J.; Peterson, B.M.; Denney, K.D.; Trump, J.R.; Sun, M.; Brandt, W.N.; Kochanek, C.S.; Dawson, K.S.; et al. The Sloan Digital Sky Survey Reverberation Mapping Project: First Broad-line Hβ and Mg II Lags at z $\gtrsim$ 0.3 from Six-month Spectroscopy. *Astrophys. J.* **2016**, *818*, 30. [CrossRef]
75. Le, H.A.N.; Woo, J.H.; Xue, Y. Calibrating Mg II-based Black Hole Mass Estimators Using Low-to-high-luminosity Active Galactic Nuclei. *Astrophys. J.* **2020**, *901*, 35. [CrossRef]
76. Yue, M.; Eilers, A.C.; Simcoe, R.A.; Mackenzie, R.; Matthee, J.; Kashino, D.; Bordoloi, R.; Lilly, S.J.; Naidu, R.P. EIGER. V. Characterizing the Host Galaxies of Luminous Quasars at z $\gtrsim$ 6. *Astrophys. J.* **2024**, *966*, 176. [CrossRef]

77. Collin-Souffrin, S. Line and continuum radiation from the outer region of accretion discs in active galactic nuclei. I-Preliminary considerations. *Astron. Astrophys.* **1987**, *179*, 60–70.
78. Marziani, P.; Sulentic, J.W.; Negrete, C.A.; Dultzin, D.; Zamfir, S.; Bachev, R. Broad-line region physical conditions along the quasar eigenvector 1 sequence. *Mon. Not. R. Astron. Soc.* **2010**, *409*, 1033–1048. [CrossRef]
79. Zamfir, S.; Sulentic, J.W.; Marziani, P.; Dultzin, D. Detailed characterization of Hβ emission line profile in low-z SDSS quasars. *Mon. Not. R. Astron. Soc.* **2010**, *403*, 1759. [CrossRef]
80. Panda, S.; Śniegowska, M. Changing-look Active Galactic Nuclei. I. Tracking the Transition on the Main Sequence of Quasars. *Astrophys. J. Suppl.* **2024**, *272*, 13. [CrossRef]
81. Komossa, S.; Grupe, D.; Marziani, P.; Popovic, L.C.; Marceta-Mandic, S.; Bon, E.; Ilic, D.; Kovacevic, A.B.; Kraus, A.; Haiman, Z.; et al. The extremes of AGN variability: Outbursts, deep fades, changing looks, exceptional spectral states, and semi-periodicities. *arXiv* **2024**, arXiv:2408.00089. [CrossRef]
82. Sulentic, J.W. Toward a classification scheme for broad-line profiles in active galactic nuclei. *Astrophys. J.* **1989**, *343*, 54–65. [CrossRef]
83. Tody, D. The IRAF Data Reduction and Analysis System. In *Proceedings of the Instrumentation in Astronomy VI*; Crawford, D.L., Ed.; Society of Photo-Optical Instrumentation Engineers (SPIE) Conference Series; SPIE: Bellingham, WA, USA 1986; Volume 627, p. 733. [CrossRef]
84. Tody, D. IRAF in the Nineties. In *Proceedings of the Astronomical Data Analysis Software and Systems II*; Hanisch, R.J., Brissenden, R.J.V., Barnes, J., Eds.; Astronomical Society of the Pacific Conference Series; Astronomical Society of the Pacific: San Francisco, CA, USA, 1993; Volume 52, p. 173.
85. Fitzpatrick, M.; Placco, V.; Bolton, A.; Merino, B.; Ridgway, S.; Stanghellini, L. Modernizing IRAF to Support Gemini Data Reduction. *arXiv* **2024**, arXiv:2401.01982. [CrossRef]
86. Kriss, G. Fitting Models to UV and Optical Spectral Data. *Astron. Data Anal. Softw. Syst. III* **1994**, *61*, 437.
87. Marziani, P.; Olmo, A.d.; Negrete, C.A.; Dultzin, D.; Piconcelli, E.; Vietri, G.; Martínez-Aldama, M.L.; D'Onofrio, M.; Bon, E.; Bon, N.; et al. The Intermediate-ionization Lines as Virial Broadening Estimators for Population A Quasars. *Astrophys. J. Suppl.* **2022**, *261*, 30. [CrossRef]
88. Zamfir, S.; Sulentic, J.W.; Marziani, P. New insights on the QSO radio-loud/radio-quiet dichotomy: SDSS spectra in the context of the 4D eigenvector1 parameter space. *Mon. Not. R. Astron. Soc.* **2008**, *387*, 856–870. [CrossRef]
89. Marziani, P.; Sulentic, J.W.; Stirpe, G.M.; Zamfir, S.; Calvani, M. VLT/ISAAC spectra of the Hβ region in intermediate-redshift quasars. III. Hβ broad-line profile analysis and inferences about BLR structure. *Astron. Astrophys.* **2009**, *495*, 83–112. [CrossRef]
90. Marziani, P.; Deconto–Machado, A.; Del Olmo, A. Isolating an Outflow Component in Single-Epoch Spectra of Quasars. *Galaxies* **2022**, *10*, 54. [CrossRef]
91. Temple, M.J. Testing AGN outflow and accretion models with SDSS quasar demographics. In *Proceedings of the IAU Symposium*; Bruni, G., Diaz Trigo, M., Laha, S., Fukumura, K., Eds.; Cambridge University Press: Cambridge, UK, 2024; Volume 378, pp. 27–29. [CrossRef]
92. Corbin, M.R. QSO Broad Emission Line Asymmetries: Evidence of Gravitational Redshift? *Astrophys. J.* **1995**, *447*, 496. [CrossRef]
93. Gavrilović, N.; Popović, L.Č.; Kollatschny, W. The gravitational redshift in the broad line region of the active galactic nucleus Mrk 110. In *Proceedings of the IAU Symposium*; Karas, V., Matt, G., Eds.; Cambridge University Press: Cambridge, UK, 2007; Volume 238, pp. 369–370. [CrossRef]
94. Jonić, S.; Kovačević-Dojčinović, J.; Ilić, D.; Popović, L.Č. Virialization of the Broad Line Region in Active Galactic Nuclei-connection between shifts and widths of broad emission lines. *Astrophys. Space Sci.* **2016**, *361*, 101. [CrossRef]
95. Bon, N.; Bon, E.; Marziani, P.; Jovanović, P. Gravitational redshift of emission lines in the AGN spectra. *Astrophys. Space Sci.* **2015**, *360*, 7. [CrossRef]
96. Heckman, T.M. An optical and radio survey of the nuclei of bright galaxies—Activity in normal galactic nuclei. *Astron. Astrophys.* **1980**, *87*, 152–164.
97. Narayan, R.; Yi, I. Advection-dominated Accretion: A Self-similar Solution. *Astrophys. J. Lett.* **1994**, *428*, L13. [CrossRef]
98. Soria, R.; Graham, A.W.; Fabbiano, G.; Baldi, A.; Elvis, M.; Jerjen, H.; Pellegrini, S.; Siemiginowska, A. Accretion and Nuclear Activity of Quiescent Supermassive Black Holes. II. Optical Study and Interpretation. *Astrophys. J.* **2006**, *640*, 143–155. [CrossRef]
99. Giustini, M.; Proga, D. A global view of the inner accretion and ejection flow around super massive black holes. Radiation-driven accretion disk winds in a physical context. *Astron. Astrophys.* **2019**, *630*, A94. [CrossRef]
100. Vestergaard, M.; Peterson, B.M. Determining Central Black Hole Masses in Distant Active Galaxies and Quasars. II. Improved Optical and UV Scaling Relationships. *Astrophys. J.* **2006**, *641*, 689–709. [CrossRef]
101. Marziani, P.; Sulentic, J.W. Evidence for a very broad line region in PG 1138+222. *Astrophys. J.* **1993**, *409*, 612–616. [CrossRef]
102. Snedden, S.A.; Gaskell, C.M. The Case for Optically Thick High-Velocity Broad-Line Region Gas in Active Galactic Nuclei. *Astrophys. J.* **2007**, *669*, 126–134. [CrossRef]

103. Marziani, P.; Dultzin-Hacyan, D.; Sulentic, J.W. Accretion onto Supermassive Black Holes in Quasars: Learning from Optical/UV Observations. In *New Developments in Black Hole Research*; Kreitler, P.V., Ed.; Nova Press: New York, NY, USA, 2006; p. 123.
104. Mineshige, S.; Kawaguchi, T.; Takeuchi, M.; Hayashida, K. Slim-Disk Model for Soft X-Ray Excess and Variability of Narrow-Line Seyfert 1 Galaxies. *Publ. Astr. Soc. Jpn.* **2000**, *52*, 499–508. [CrossRef]
105. Sądowski, A. Slim Disks Around Kerr Black Holes Revisited. *Astrophys. J. Suppl.* **2009**, *183*, 171–178. [CrossRef]
106. Dotan, C.; Shaviv, N.J. Super-Eddington slim accretion discs with winds. *Mon. Not. R. Astron. Soc.* **2011**, *413*, 1623–1632. [CrossRef]
107. Abramowicz, M.A.; Straub, O. Accretion discs. *Scholarpedia* **2014**, *9*, 2408. [CrossRef]
108. Romero, G.E.; Abraham, Z. Precession of relativistic jets in active galactic nuclei as a clue to binary supermassive black holes. *Int. J. Mod. Phys. D* **2000**, *9*, 173–184. [CrossRef]
109. Krause, M.; Burkert, A.; Schartmann, M. Stability of cloud orbits in the broad-line region of active galactic nuclei. *Mon. Not. R. Astron. Soc.* **2011**, *411*, 550–556. [CrossRef]
110. Decarli, R.; Dotti, M.; Treves, A. Geometry and inclination of the broad-line region in blazars. *Mon. Not. R. Astron. Soc.* **2011**, *413*, 39–46. [CrossRef]
111. Afanasiev, V.L.; Popović, L.Č.; Shapovalova, A.I. Spectropolarimetry of Seyfert 1 galaxies with equatorial scattering: Black hole masses and broad-line region characteristics. *Mon. Not. R. Astron. Soc.* **2019**, *482*, 4985–4999. [CrossRef]
112. Wills, B.J.; Browne, I.W.A. Relativistic beaming and quasar emission lines. *Astrophys. J.* **1986**, *302*, 56–63. [CrossRef]
113. Marin, F. Are there reliable methods to estimate the nuclear orientation of Seyfert galaxies? *Mon. Not. R. Astron. Soc.* **2016**, *460*, 3679–3705. [CrossRef]
114. Punsly, B.; Tramacere, A.; Kharb, P.; Marziani, P. The Powerful Jet and Gamma-Ray Flare of the Quasar PKS 0438–436. *Astrophys. J.* **2018**, *869*, 174. [CrossRef]
115. Marziani, P.; Bon, E.; Bon, N.; D'Onofrio, M.; Punsly, B.; Śniegowska, M.; Czerny, B.; Panda, S.; Martínez Aldama, M.L.; del Olmo, A.; et al. The main sequence of quasars: The taming of the extremes. *Astron. Nachrichten* **2022**, *343*, e210082. [CrossRef]
116. Lynden-Bell, D. Galactic Nuclei as Collapsed Old Quasars. *Nature* **1969**, *223*, 690–694. [CrossRef]
117. Lin, D.N.C.; Papaloizou, J. On the Tidal Interaction between Protoplanets and the Protoplanetary Disk. III. Orbital Migration of Protoplanets. *Astrophys. J.* **1986**, *309*, 846. [CrossRef]
118. Artymowicz, P.; Lubow, S.H. Dynamics of Binary-Disk Interaction. I. Resonances and Disk Gap Sizes. *Astrophys. J.* **1994**, *421*, 651. [CrossRef]
119. Tiede, C.; Zrake, J.; MacFadyen, A.; Haiman, Z. How Binaries Accrete: Hydrodynamic Simulations with Passive Tracer Particles. *Astrophys. J.* **2022**, *932*, 24. [CrossRef]
120. Chen, K.; Halpern, J.P.; Filippenko, A.V. Kinematic evidence for a relativistic Keplerian disk-ARP 102B. *Astrophys. J.* **1989**, *339*, 742–751. [CrossRef]
121. Eracleous, M.; Halpern, J.P. Completion of a Survey and Detailed Study of Double-peaked Emission Lines in Radio-loud Active Galactic Nuclei. *Astrophys. J.* **2003**, *599*, 886–908. [CrossRef]
122. Strateva, I.V.; Strauss, M.A.; Hao, L.; Schlegel, D.J.; Hall, P.B.; Gunn, J.E.; Li, L.; Ivezić, Ž.; Richards, G.T.; Zakamska, N.L.; et al. Double-peaked Low-Ionization Emission Lines in Active Galactic Nuclei. *Astron. J.* **2003**, *126*, 1720–1749. [CrossRef]
123. Mengistue, S.T.; Del Olmo, A.; Marziani, P.; Pović, M.; Martínez-Carballo, M.A.; Perea, J.; Márquez, I. Optical and near-UV spectroscopic properties of low-redshift jetted quasars in the main sequence context. *Mon. Not. R. Astron. Soc.* **2023**, *525*, 4474–4496. [CrossRef]
124. Peters, P.C. Gravitational Radiation and the Motion of Two Point Masses. *Phys. Rev.* **1964**, *136*, 1224–1232. [CrossRef]
125. Deng, H. Gravitational wave background from mergers of large primordial black holes. *J. Cosmol. Astropart. Phys.* **2022**, *2022*, 037. [CrossRef]
126. Nguyen, K.; Bogdanović, T. Emission Signatures from Sub-parsec Binary Supermassive Black Holes. I. Diagnostic Power of Broad Emission Lines. *Astrophys. J.* **2016**, *828*, 68. [CrossRef]
127. Hobbs, G.; Archibald, A.; Arzoumanian, Z.; Backer, D.; Bailes, M.; Bhat, N.D.R.; Burgay, M.; Burke-Spolaor, S.; Champion, D.; Cognard, I.; et al. The International Pulsar Timing Array project: Using pulsars as a gravitational wave detector. *Class. Quantum Gravity* **2010**, *27*, 084013. [CrossRef]
128. Mingarelli, C.M.F.; Lazio, T.J.W.; Sesana, A.; Greene, J.E.; Ellis, J.A.; Ma, C.P.; Croft, S.; Burke-Spolaor, S.; Taylor, S.R. The local nanohertz gravitational-wave landscape from supermassive black hole binaries. *Nat. Astron.* **2017**, *1*, 886–892. [CrossRef]
129. Antonini, F.; Perets, H.B. Secular Evolution of Compact Binaries near Massive Black Holes: Gravitational Wave Sources and Other Exotica. *Astrophys. J.* **2012**, *757*, 27. [CrossRef]
130. Wang, J.M.; Yan, C.S.; Li, Y.R.; Chen, Y.M.; Xiang, F.; Hu, C.; Ge, J.Q.; Zhang, S. Evolution of Gaseous Disk Viscosity Driven by Supernova Explosions in Star-Forming Galaxies at High Redshift. *Astrophys. J. Lett.* **2009**, *701*, L7–L11. [CrossRef]
131. Wang, J.; Deng, J.S.; Wei, J.Y. Ongoing star formation in AGN host galaxy discs: A view from core-collapse supernovae. *Mon. Not. R. Astron. Soc.* **2010**, *405*, 2529–2533. [CrossRef]

132. Wang, J.M.; Ge, J.Q.; Hu, C.; Baldwin, J.A.; Li, Y.R.; Ferland, G.J.; Xiang, F.; Yan, C.S.; Zhang, S. Star Formation in Self-gravitating Disks in Active Galactic Nuclei. I. Metallicity Gradients in Broad-line Regions. *Astrophys. J.* **2011**, *739*, 3. [CrossRef]
133. Wang, J.M.; Du, P.; Baldwin, J.A.; Ge, J.Q.; Hu, C.; Ferland, G.J. Star Formation in Self-gravitating Disks in Active Galactic Nuclei. II. Episodic Formation of Broad-line Regions. *Astrophys. J.* **2012**, *746*, 137. [CrossRef]
134. Artymowicz, P.; Lin, D.N.C.; Wampler, E.J. Star Trapping and Metallicity Enrichment in Quasars and Active Galactic Nuclei. *Astrophys. J.* **1993**, *409*, 592. [CrossRef]
135. Lin, D.N.C. Star/Disk Interaction in the Nuclei of Active Galaxies. In *Proceedings of the IAU Colloq. 159: Emission Lines in Active Galaxies: New Methods and Techniques*; Peterson, B.M., Cheng, F.Z., Wilson, A.S., Eds.; Astronomical Society of the Pacific Conference Series; Astronomical Society of the Pacific: San Francisco, CA, USA, 1997; Volume 113, p. 64.
136. Collin, S.; Zahn, J.P. Star formation and evolution in accretion disks around massive black holes. *Astron. Astrophys.* **1999**, *344*, 433–449.
137. Wang, J.M.; Zhai, S.; Li, Y.R.; Songsheng, Y.Y.; Ho, L.C.; Chen, Y.J.; Liu, J.R.; Du, P.; Yuan, Y.F. Star Formation in Self-gravitating Disks in Active Galactic Nuclei. III. Efficient Production of Iron and Infrared Spectral Energy Distributions. *Astrophys. J.* **2023**, *954*, 84. [CrossRef]
138. Dittmann, A.J.; Cantiello, M. A Semi-Analytical Model for Stellar Evolution in AGN Disks. *arXiv* **2024**, arXiv:2409.02981. [CrossRef]
139. Fabj, G.; Dittmann, A.J.; Cantiello, M.; Perna, R.; Samsing, J. Mapping the Outcomes of Stellar Evolution in the Disks of Active Galactic Nuclei. *arXiv* **2024**, arXiv:2408.16050. [CrossRef]
140. Liu, J.R.; Wang, Y.L.; Wang, J.M. Accretion-modified Stars in Accretion Disks of Active Galactic Nuclei: Observational Characteristics in Different Regions of the Disks. *Astrophys. J.* **2024**, *969*, 37. [CrossRef]
141. Fraix-Burnet, D.; Marziani, P.; D'Onofrio, M.; Dultzin, D. The Phylogeny of Quasars and the Ontogeny of Their Central Black Holes. *Front. Astron. Space Sci.* **2017**, *4*, 1. [CrossRef]
142. Elitzur, M.; Shlosman, I. The AGN-obscuring Torus: The End of the "Doughnut" Paradigm? *Astrophys. J. Lett.* **2006**, *648*, L101–L104. [CrossRef]
143. Portegies Zwart, S.F.; McMillan, S.L.W. The Runaway Growth of Intermediate-Mass Black Holes in Dense Star Clusters. *Astrophys. J.* **2002**, *576*, 899–907. [CrossRef]
144. Portegies Zwart, S.F.; Baumgardt, H.; Hut, P.; Makino, J.; McMillan, S.L.W. Formation of massive black holes through runaway collisions in dense young star clusters. *Nature* **2004**, *428*, 724–726. [CrossRef] [PubMed]
145. Gaete, B.; Schleicher, D.R.G.; Lupi, A.; Reinoso, B.; Fellhauer, M.; Vergara, M.C. Supermassive black hole formation via collisions in black hole clusters. *Astron. Astrophys.* **2024**, *690*, A378. [CrossRef]
146. Chen, Y.X.; Lin, D.N.C. The Population of Massive Stars in Active Galactic Nuclei Disks. *Astrophys. J.* **2024**, *967*, 88. [CrossRef]
147. Neumayer, N.; Seth, A.; Böker, T. Nuclear star clusters. *Astron. Astrophys. Rev.* **2020**, *28*, 4. [CrossRef]
148. Böker, T. Nuclear star clusters. In *Proceedings of the Star Clusters: Basic Galactic Building Blocks Throughout Time and Space*; de Grijs, R., Lépine, J.R.D., Eds.; IAU Symposium; Cambridge University Press: Cambridge, UK, 2010; Volume 266, pp. 58–63. [CrossRef]
149. Tagawa, H.; Haiman, Z.; Kocsis, B. Formation and Evolution of Compact-object Binaries in AGN Disks. *Astrophys. J.* **2020**, *898*, 25. [CrossRef]
150. Barack, L.; Cardoso, V.; Nissanke, S.; Sotiriou, T.P.; Askar, A.; Belczynski, C.; Bertone, G.; Bon, E.; Blas, D.; Brito, R.; et al. Black holes, gravitational waves and fundamental physics: A roadmap. *Class. Quantum Gravity* **2019**, *36*, 143001, [CrossRef]
151. Abbott, B.P.; Abbott, R.; Abbott, T.D.; Abernathy, M.R.; Acernese, F.; Ackley, K.; Adams, C.; Adams, T.; Addesso, P.; Adhikari, R.X.; et al. Observation of Gravitational Waves from a Binary Black Hole Merger. *Phys. Rev. Lett.* **2016**, *116*, 061102. [CrossRef]
152. Ebisuzaki, T.; Makino, J.; Tsuru, T.G.; Funato, Y.; Portegies Zwart, S.; Hut, P.; McMillan, S.; Matsushita, S.; Matsumoto, H.; Kawabe, R. Missing Link Found? The "Runaway" Path to Supermassive Black Holes. *Astrophys. J. Lett.* **2001**, *562*, L19–L22. [CrossRef]
153. Mapelli, M. Massive black hole binaries from runaway collisions: The impact of metallicity. *Mon. Not. R. Astron. Soc.* **2016**, *459*, 3432–3446. [CrossRef]
154. Belczynski, K.; Bulik, T.; Fryer, C.L.; Ruiter, A.; Valsecchi, F.; Vink, J.S.; Hurley, J.R. On the Maximum Mass of Stellar Black Holes. *Astrophys. J.* **2010**, *714*, 1217–1226. [CrossRef]
155. Giacobbo, N.; Mapelli, M. The progenitors of compact-object binaries: Impact of metallicity, common envelope and natal kicks. *Mon. Not. R. Astron. Soc.* **2018**, *480*, 2011–2030. [CrossRef]
156. Gröbner, M.; Ishibashi, W.; Tiwari, S.; Haney, M.; Jetzer, P. Binary black hole mergers in AGN accretion discs: Gravitational wave rate density estimates. *Astron. Astrophys.* **2020**, *638*, A119. [CrossRef]
157. Wang, J.M.; Liu, J.R.; Ho, L.C.; Li, Y.R.; Du, P. Accretion-modified Stars in Accretion Disks of Active Galactic Nuclei: Gravitational-wave Bursts and Electromagnetic Counterparts from Merging Stellar Black Hole Binaries. *Astrophys. J. Lett.* **2021**, *916*, L17. [CrossRef]
158. Jermyn, A.S.; Dittmann, A.J.; McKernan, B.; Ford, K.E.S.; Cantiello, M. Effects of an Immortal Stellar Population in AGN Disks. *Astrophys. J.* **2022**, *929*, 133. [CrossRef]

159. Sicilia, A.; Lapi, A.; Boco, L.; Spera, M.; Di Carlo, U.N.; Mapelli, M.; Shankar, F.; Alexander, D.M.; Bressan, A.; Danese, L. The Black Hole Mass Function Across Cosmic Times. I. Stellar Black Holes and Light Seed Distribution. *Astrophys. J.* **2022**, *924*, 56. [CrossRef]
160. LIGO Scientific Collaboration; Aasi, J.; Abbott, B.P.; Abbott, R.; Abbott, T.; Abernathy, M.R.; Ackley, K.; Adams, C.; Adams, T.; Addesso, P.; et al. Advanced LIGO. *Class. Quantum Gravity* **2015**, *32*, 074001. [CrossRef]
161. Acernese, F.; Agathos, M.; Agatsuma, K.; Aisa, D.; Allemandou, N.; Allocca, A.; Amarni, J.; Astone, P.; Balestri, G.; Ballardin, G.; et al. Advanced Virgo: A second-generation interferometric gravitational wave detector. *Class. Quantum Gravity* **2015**, *32*, 024001. [CrossRef]
162. Punturo, M.; Abernathy, M.; Acernese, F.; Allen, B.; Andersson, N.; Arun, K.; Barone, F.; Barr, B.; Barsuglia, M.; Beker, M.; et al. The Einstein Telescope: A third-generation gravitational wave observatory. *Class. Quantum Gravity* **2010**, *27*, 194002. [CrossRef]
163. Maggiore, M.; Van Den Broeck, C.; Bartolo, N.; Belgacem, E.; Bertacca, D.; Bizouard, M.A.; Branchesi, M.; Clesse, S.; Foffa, S.; García-Bellido, J.; et al. Science case for the Einstein telescope. *J. Cosmol. Astropart. Phys.* **2020**, *2020*, 050. [CrossRef]

Disclaimer/Publisher's Note: The statements, opinions and data contained in all publications are solely those of the individual author(s) and contributor(s) and not of MDPI and/or the editor(s). MDPI and/or the editor(s) disclaim responsibility for any injury to people or property resulting from any ideas, methods, instructions or products referred to in the content.